HHS Public Access

Author manuscript

NMR Biomed. Author manuscript; available in PMC 2017 December 15.

Published in final edited form as:

NMR Biomed. 2014 October ; 27(10): 1159–1166. doi:10.1002/nbm.3169.

Characterization of trabecular bone density with ultra-short echo-time MRI at 1.5, 3.0 and 7.0 T – comparison with micro-computed tomography

Moritz C. Wurnig[a,*], **Maurizio Calcagni**[b], **David Kenkel**[a], **Magdalena Vich**[c], **Markus Weiger**[d], **Gustav Andreisek**[a], **Felix W. Wehrli**[e], and **Andreas Boss**[a]

[a]Department of Diagnostic and Interventional Radiology, University Hospital Zurich, Switzerland [b]Division of Plastic and Reconstructive Surgery, University Hospital Zurich, Switzerland [c]Institute of Anatomy, University of Zurich, Switzerland [d]Institute for Biomedical Engineering, University and ETH Zurich, Switzerland [e]Laboratory for Structural NMR Imaging, Department of Radiology, Perelman School of Medicine, University of Pennsylvania, USA

Abstract

The goal of this study was to test the potential of ultra-short echo-time (UTE) MRI at 1.5, 3.0 and 7.0 T for depiction of trabecular bone structure (of the wrist bones), to evaluate whether T_2* relaxation times of bone water and parametric maps of T_2* of trabecular bone could be obtained at all three field strengths, and to compare the T_2* relaxation times with structural parameters obtained from micro-computed tomography (micro-CT) as a reference standard. *Ex vivo* carpal bones of six wrists were excised *en bloc* and underwent MRI at 1.5, 3.0 and 7.0 T in a whole-body MR imager using the head coil. A three-dimensional radial fat-suppressed UTE sequence was applied with subsequent acquisitions, with six different echo times T_E of 150, 300, 600, 1200, 3500 and 7000 μs. The T_2* relaxation time and pixel-wise computed T_2* parametric maps were compared with a micro-computed-tomography reference standard providing trabecular bone structural parameters including porosity (defined as the bone-free fraction within a region of interest), trabecular thickness, trabecular separation, trabecular number and fractal dimension (D_k). T_2* relaxation curves and parametric maps could be computed from datasets acquired at all field strengths. Mean T_2* relaxation times of trabecular bone were 4580 ± 1040 μs at 1.5T, 2420 ± 560 μs at 3.0 T and 1220 ± 300 μs at 7.0 T, when averaged over all carpal bones. A positive correlation of T_2* with trabecular bone porosity and trabecular separation, and a negative correlation of T_2* relaxation time with trabecular thickness, trabecular number and fractal dimension, was detected ($p < 0.01$ for all field strengths and micro-CT parameters). We conclude that UTE MRI may be useful to characterize the structure of trabecular bone, comparable to micro-CT.

*Correspondence to: M. C. Wurnig, Department of Diagnostic and Interventional Radiology, University Hospital Zurich, Switzerland. moritz.wurnig@usz.ch.

Keywords

relaxometry; endogenous contrast methods; methods and engineering; quantitation; post-acquisition processing; methods and engineering; bone; musculoskeletal; applications

INTRODUCTION

Rheumatoid arthritis is a progressive systemic disease, which can affect all small and large joints and can lead to severe motion impairment. Signs of rheumatoid arthritis include bone erosions around the joint as well as periarticular osteoporosis (1). The most common affected joints include the metacarpophalangeal, proximal interphalangeal and wrist joints (2,3), and a decrease in bone density of the hand is often noted (4). Only recently, it could be shown that a decrease in bone density in this patient cohort is also associated with joint destruction (5), and thus measurement of periarticular osteoporosis has been proposed to monitor treatment effects in rheumatoid arthritis (6).

The radiological gold standard for visualization of the trabecular bone structure is micro-computed tomography (micro-CT), providing resolutions in the range of 18–82 μm (7,8), which is well below the size of typical trabecular structures, of the order of 100 μm. However, the application of micro-CT is limited to bone biopsy cores, *ex vivo* samples and animal experimentation. For patient monitoring, a technique for bone characterization not relying on ionizing irradiation would be highly desirable.

Several MRI techniques have been described that are able to provide a characterization of trabecular bone (9–11). Many of these techniques rely on the measurement of T_2* relaxation properties of trabecular bone marrow. The magnetic susceptibility difference between trabecular bone and bone marrow results in mesoscopic magnetic field inhomogeneities causing rapid signal dephasing and a short T_2* time. The relaxation times, thereby, indirectly provide information on bone microstructure (12–14). As susceptibility effects linearly scale with the static magnetic field, in principle, elevated field strength may provide not only superior signal to noise but also improved characterization of trabecular bone structure.

One obstacle for the direct application of MRI techniques for characterization of bone tissue itself is the extremely rapid signal decay, which precludes the depiction of bone structures with conventional MRI sequences with echo times (T_E) of 2–10 ms. The introduction of MRI sequences with ultra-short echo time (UTE, 100 μs and below) and radial *k*-space sampling allowed for the first time direct visualization of trabecular and cortical bone (15). Furthermore, these sequences allow direct assessment and quantification of T_2* relaxation properties of the water protons in bone tissue (16,17). This sequence type becomes particularly important in ultra-high field MRI due to the even faster decay of the transverse magnetization. A successful implementation of a UTE sequence at 7.0 T has just recently been reported (18).

The purpose of this study was to test the ability of UTE sequences at 1.5, 3.0 and 7.0 T to depict trabecular bone structure (of the wrist bones), to evaluate whether T_2* of bone water

protons and parametrical maps of T_2* time of trabecular bone could be obtained at all three field strengths, and to compare the T_2* relaxation time of trabecular bone acquired via UTE MRI at different field strengths with structural parameters obtained from micro-CT as a reference standard. We note that, unlike prior work exploiting the susceptibility differences between bone and marrow (see, for example, Wehrli *et al.* (19) for a review of the subject) by quantifying the signal decay of bone marrow protons, in this work we evaluate T_2* of the short-lived water protons in the bone itself and therefore provide a more direct approach, which is also potentially less affected by possible alterations of bone marrow.

MATERIAL AND METHODS

Specimens

For this study, six Thiel-fixated wrists (four left, two right, four donors, three male, mean age 65 years, range 50–74 years) were obtained from the Anatomical Institute of the University of Zurich. Thiel fixation, as introduced by Thiel (20,21), is an almost odorless embalming method, which although containing certain amounts of formalin and ethyl alcohol, avoids unnatural effects such as hardening, contractions or swelling of the tissue and provides furthermore good conservation of color as well as a good disinfection effect. Prior to imaging, the carpal bones of the wrists were excised *en bloc*, while not touching the intrinsic ligaments to keep the situs as original as possible. Major degeneration of the carpal bones was ruled out visually. Between imaging sessions, all specimens were wrapped in gauze soaked with Thiel solution and stored cooled at 4 °C. For the scans, the specimens were unwrapped and placed without a special covering.

According to local regulations and laws, cantonal ethics board approval was not required for this prospective human cadaver study. The institutional review board approved this study, which was conducted according to the Declaration of Helsinki. All cadaveric specimens were treated in accordance with the university’s and institution’s regulations on cadaveric studies.

MRI

MRI was performed on a 1.5 T Philips Achieva (Best, The Netherlands), a 3.0 T Philips Ingenia and a 7.0 T Philips Achieva system. At 1.5 and 3.0 T an eight-channel head coil and at 7.0 T a 32-channel head coil were used. After gradient-echo localizers in three spatial directions, the imaging protocol comprised a coronal and a transversal T_1 weighted fast spin echo sequence (T_E 22 ms, T_R 557 ms, turbo factor 3, field of view (FOV) 80 × 80 × 46, mm^3, matrix 268 × 199, slices 12, number of acquisitions 12) for further planning of the study. To measure T_2*, a three-dimensional radial UTE sequence was applied by collecting echoes at T_E of 150, 300, 600, 1200, 3500 and 7000 μs. Here, T_E denotes the time between the RF pulse end and the start of acquisition/gradient ramp. Different T_E values were acquired in subsequent scans while keeping adjusted parameters such as receiver gain and RF power unchanged. To eliminate signal from bone marrow and thus its effect on T_2*, a SPIR (spectral presaturation with inversion recovery) fat saturation prepulse (flip angle 120°, off-resonance −4.1 ppm) (22) was applied before each UTE excitation. Global first-order shimming was used to provide sufficient B_0 homogeneity for a satisfactory performance of

the SPIR pulse. Other parameters of the UTE sequence included repetition time T_R 34 ms, matrix 116 × 116 × 116, FOV 70 × 70 × 70 mm^3, spatial resolution 0.6 × 0.6 × 0.6 mm^3, flip angle 15.0°, duration of non-selective block pulse 40–70 μs, pixel bandwidth 539/575/1026 Hz (for 1.5/3.0/7.0 T), readout duration 1045/715/624 μs (for 1.5/3.0/7.0 T), gradient ramp duration 117/132/200 μs (for 1.5/3.0/7.0 T), number of acquisitions 1, and acquisition time 40 min 27 s per echo for all field strengths. All scan parameters for the UTE sequence were kept the same at the different field strengths.

Micro-CT imaging

For micro-CT imaging, a SkyScan 1176 system (Bruker-microCT, Kontich, Belgium) was used. Specimens were placed on the mouse bed, and after an initial localizer scan images were acquired using the following scan parameters: tube voltage 90 kV, tube current 280 μA, exposure time 65 ms, rotation step 0.7°, covered angle 360°, copper filter 0.1 mm, voxel size 35 × 35 × 35 μm^3, FOV 68 × 68 × 20 mm^3, frame averaging 3. To cover the whole specimens, multiple overlapping scans were performed and the acquired images were fused using the reconstruction software of the manufacturer. The duration of one scan was 50–70 min depending on the maximal transverse diameter of the scanned specimen. Images were then reconstructed using a modified Feldkamp algorithm with the following parameters: beam hardening correction 35%, ring artifact reduction 6, Gaussian smoothing kernel with full width at half maximum of 4 voxels.

Data analysis

Prior to data analysis, MR images acquired at the different field strengths were coregistered for each specimen. For coregistration, the' coregister & reslice' function of the statistical parametric mapping MATLAB toolbox (SPM8, Wellcome Department of Cognitive Neurology, London, UK) was used. Due to memory constraints of the hardware used, micro-CT data with a lowered resolution (70 μm instead of 35 μm) were then coregistered to the respective MR images in the same way. To preserve the acquired resolution, finally the originally acquired micro-CT data were manually coregistered to these automatically coregistered micro-CT data with lowered resolution.

To measure the T_2* decay of trabecular bone as well as the structural parameters acquired via micro-CT (porosity, trabecular thickness, trabecular separation, trabecular number, fractal dimension), matching regions of interest (ROIs) were drawn on the MR images acquired at 1.5 T and the coregistered micro-CT images. For 3.0 and 7.0 T, the same ROIs were copied to the respective data sets as applied for 1.5 T. For each carpal bone one ROI containing the central trabecular zone as well as one ROI containing the peripheral trabecular zone were drawn on three slices (proximal, central and distal), resulting in 288 ROIs in total.

The T_2* time constant was computed by fitting the mean signal intensities within the ROIs at the given echo times to the following model for a mono-exponential decay:

$$S(t)=S_0 \times \mathrm{e}^{-t/T2^*}+N.$$

The fitting routine used a nonlinear least-squares fit with an algorithm based on the interior-reflective Newton method, and S_0 and the T_2* time constant were used as fitting variables. The noise term N was not fitted, but estimated as the standard deviation in a ROI selected in the image background outside the object avoiding regions masked due to the radial acquisition, which resulted in greater stability of fit parameters.

The frequency distribution within ROIs was calculated by a discrete fast Fourier transform of the measured signal intensity values for the six different T_E values. Before Fourier transformation, the data were interpolated using piecewise cubic Hermite interpolating polynomials to an equidistant grid and zero-filled up to 1024 points.

From micro-CT images, the following structural parameters based on the nomenclature and definition by Parfitt *et al.* (23) were computed within the ROIs to characterize the trabecular bone structure: porosity of the trabecular bone (Po), trabecular thickness (Tr.Th), trabecular separation (Tr.Se) and trabecular number (Tr.N). As a marker of the two-dimensional architectural complexity of trabecular bone, which has also been shown to exhibit a correlation to physical properties (24–26), the fractal dimension (D_k) was computed based on the Kolmogorov method as described by Chappard *et al.* (27). In this method, grids of varying sizes are superimposed on the analyzed trabecular structure. Then the number of intersecting grid boxes is counted. Finally, the number of intersecting boxes is plotted against the length of one box on a log–log graph and the fractal dimension is computed as the slope of the linear regression.

Statistical analysis

For statistical analysis, mean values and standard deviations were computed. All variables were examined for normality with the Kolmogorov–Smirnov test. Depending on the result of the test a one way ANOVA or a Kruskal–Wallis test was used to test for a statistically significant difference of variables between ROIs within the different carpal bones. If a statistically significant difference could be detected, a Bonferroni or Dunn *post hoc* analysis followed. Further, Pearson or Spearman correlation coefficients were calculated to assess correlations between T_2* time and structural parameters obtained via micro-CT.

All p-values less than 0.05 were considered to be statistically significant. All statistical analyses were performed by using commercially available software (GraphPad Prism version 5.04 for Windows, GraphPad Software, La Jolla, CA, USA).

RESULTS

MRI

Radial UTE sequences showed high signal intensity for cartilage, low signal intensity for cortical bone and a signal intensity in-between cartilage and cortical bone for trabecular bone (Fig. 1).

Mean T_2* relaxation times (Figs. 2 and 3) of trabecular bone were 4590 ± 1040 μs at 1.5 T, 2420 ± 560 μs at 3.0 T and 1220 ± 300 μs at 7.0 T, when averaged over all carpal bones. When comparing the T_2* relaxation time of the individual carpal bones at 1.5 T the

following pattern was observed: trapezium, trapezoid and pisiform showed the longest T_2* times, while scaphoid, lunate, capitate and hamate exhibited the shortest T_2* times and T_2* times of triquetrum lay in between. Most of the differences between the bones with long T_2* times and the bones with short T_2* times were statistically significant (cf. Table 1). While these differences were also observed at 3.0 and 7.0 T, not all of them were statistically significant (cf. Table 1).

FWHM values of the frequency distributions within the ROIs showed an increase with field strength, as shown for exemplary data in Fig. 4.

Micro-CT imaging

Images acquired with micro-CT showed an excellent depiction of cortical and trabecular bone (Fig. 1). Trabecular bone exhibited a mean porosity of 61.8 ± 9.7%, a mean trabecular thickness of 214 ± 37 μm, a mean trabecular separation of 381 ± 140 μm, a mean trabecular number of 1.96 ± 0.36 mm^{-1} and a mean fractal dimension of 1.53 ± 0.09 when averaged over all carpal bones.

When comparing the structural parameters of the individual carpal bones a pattern corresponding to the T_2* time pattern was observed: While trapezium, trapezoid and pisiform showed the highest porosity and trabecular separation, the corresponding numbers for the scaphoid, lunate, capitate and hamate were the lowest and the triquetrum lay between the two groups. Similar to T_2* time, not all but most of the differences between the bones showing high porosity and trabecular separation and the bones exhibiting low porosity and trabecular separation were statistically significant (cf. Table 2). For trabecular thickness, trabecular number and fractal dimension, the pattern was inverted.

Correlation analysis

Correlation analysis showed a moderate correlation between T_2* time and almost all assessed structural parameters of trabecular bone. While the 3.0 T data in absolute values mostly showed the highest correlation to micro-CT data, 1.5 and 7.0 T data performed almost equally. In particular, the comparison between T_2* relaxation time and structural parameters of trabecular bone revealed a positive correlation of T_2* with porosity (1.5 T, R = 0.52; 3.0 T, 0.57; 7.0 T, 0.50) and trabecular separation (1.5 T, R = 0.39; 3.0 T, 0.53; 7.0 T, 0.44). A negative correlation of T_2* relaxation time was observed with trabecular thickness (1.5 T, R = −0.47; 3.0 T, −0.39; 7.0 T, −0.44), trabecular number (1.5 T, R = −0.14; 3.0 T, −0.41; 7.0 T, −0.31) and fractal dimension (1.5 T, R = −0.45; 3.0 T, −0.47; 7.0 T, −0.41) (Fig. 5). Except for trabecular number at 1.5 T, with a p-value of 0.01, all correlations were highly significant, with $p < 0.0001$.

DISCUSSION

In the present study, we were able to show that carpal bony structures – a site that is commonly affected in patients with rheumatoid arthritis – may be depicted at 1.5, 3.0 and 7.0 T using UTE sequences with 3D radial k-space sampling. In spite of the notably faster signal decay at increasing field strength, T_2* relaxation times and T_2* parametric maps of acceptable image quality could be computed at all field strengths. The obtained relaxation

times at all field strengths exhibited statistically significant correlations with the respective parameters from the micro-CT reference standard.

Structural analysis of trabecular bone via CT has been proven a valuable tool to monitor disease progression and treatment response as well as to evaluate the risk of complications, not only for rheumatoid arthritis but also for a range of diseases such as osteoporosis, osteoarthritis and diabetes (28–35). Still, structural analysis via CT is a research topic and not yet part of clinical radiology. Furthermore, assessment via MRI might be advantageous not only because of the absence of ionizing irradiation, which is predominantly a concern in young or pediatric patients (for instance patients with renal insufficiency suffering from reduced bone density) but also because MRI offers the possibility to acquire additional information regarding the metabolic status of the tissue, for instance bone perfusion, which is known to be related to bone remodeling (36–41).

In principle, elevated field strength is advantageous, especially for imaging of the musculoskeletal system. The reason for this is the higher signal-to-noise ratio, which in theory linearly increases with the field strength, the applicability of dedicated transmit–receive coils less limited by restrictions due to energy deposition by the B_1 field, and the B_1 field homogeneity being superior to that for imaging larger anatomic structures such as the abdomen or chest. The feasibility of T_2* measurements with UTE MRI to assess trabecular bone structure at high field strengths is particularly promising, as susceptibility effects scale with B_0 and therefore smaller differences in trabecular structure might be detected with greater sensitivity. Furthermore, MRI at field strengths greater than 3.0 T is still in its infancy when compared with the broad experience that exists and the technical advances achieved at field strengths of 1.5 and 3.0 T. Together with the relative lack of dedicated coils for imaging of extremities at 7.0 T, further advances are expected in the near future, thereby making ultra-high field MRI increasingly attractive in the clinic.

The T_2* obtained shortens with increasing trabecular density, i.e. when the trabecular structure approaches that of a solid akin to cortical bone. The correlation between T_2* relaxation time and structural parameters could be observed well for the individual analysis of the carpal bones, where corresponding patterns could be found considering that only six specimens without notable pathological alterations of the bone density have been evaluated. Higher correlation coefficients could potentially have been obtained from a larger set of specimens exhibiting a greater variability of physiological and pathological bone density. Interestingly, correlation coefficients were highest for the 3.0 T data, whereas 1.5 T and 7.0 T data showed rather similar correlation coefficients. We hypothesize that this could be due to the increasing susceptibility effects leading to increased sensitivity to detect varying trabecular structure for 3.0 T when compared to 1.5 T, but also leading to increased variability of measurement points at 7.0 T when compared to 3.0 T.

It is known that water within the bone resides in different compartments: bound to crystal structure, collagen and residing within the Haversian canal system and bone marrow pores. In recent years UTE MRI has been used to study bone water extensively, and quantification of bone water within the Haversian canal system was reported for cortical bone (42–45). The results of our T_2* measurements in trabecular bone as well as the correlation to structural

parameters is in good agreement with previous reports with UTE spectroscopic imaging and UTE MRI in cortical bone, where similar T_2* times for free water as well as a correlation with structural parameters were found (46,47). Although the correlation of T_2* values for free water to porosity was, in contrast to our results, not significant (probably due to the low variation of porosity in cortical bone), a significant correlation to biomechanical measures was reported (46). However, we cannot completely rule out that the measured values with the present approach were dominated by water within bone marrow pores (similar to the approach of De Santis *et al.* (48)) or olefinic protons in triglycerides (which have a chemical shift close to water and might not be completely suppressed). To assess this issue, a multi-exponential analysis of the signal decay to separate the different contributing spin components could be used, for instance. Due to the low number of acquired echoes, this approach is not applicable in this study, and therefore this is reserved for future studies with an acquisition of a large number of different echoes. Another effect that might have an influence is a phase shift of the water signal due to the magnetic susceptibility difference between bone water and bone marrow fat (49,50). All the effects discussed above might have added variability to the measured T_2* values, resulting in the observed moderate correlation coefficients.

Our study has limitations. First, the number of specimens was low. To partly overcome this limitation, a large number of ROIs with representative and varying tissue properties was examined. Second, the use of fixated wrists might lead to biased results due to the fixation. Although fresh frozen specimen would have been preferable and some studies have reported changes in some mechanical properties of bone (but not in bone mineral density) due to Thiel fixation (51,52), there was no evidence of structural abnormalities in the micro-CT images. Third, the acquisition times for UTE MRI currently render the method impractical for clinical use. The long acquisition times are the result of the relatively long pulse repetition time, which was kept constant for all T_E values and field strengths to keep systematic variability as low as possible. T_R was constrained by the application of the SPIR pulse and by the specific absorption rate (SAR) associated with the latter as well as the excitation pulse. To reduce scan time, a SPIR pulse could be followed by multiple UTE acquisitions, thus reducing T_R and also SAR constraints by minimizing the number of SPIR pulses and reduced excitation flip angles. However, this modification would generally lead to worse fat suppression, and thereby would result in accuracy loss for the measurement of bone water T_2*. To reduce total scan time per T_E series acquisition of multiple echoes per excitation could be used. Other approaches that lower scan time are also feasible, including parallel imaging or lowering of resolution. As a fourth limitation of our study, the final step of the coregistration of the UTE MR and micro-CT datasets was carried out manually, probably resulting in some added variability. A completely automated coregistration would have been preferable, but was in this case technically not feasible due to memory limitations of the available hardware. Finally, although we tried to avoid the development of air filled spaces as far as possible (which typically occur if the sample is preserved for some time), this was not possible in all cases. CT scans were always acquired last, as influence by air is far less severe than with MRI. Although we tried to avoid such areas in our analysis, some ROIs might be influenced by air.

We conclude that UTE MRI can be used to characterize the structure of trabecular bone, and although assessing trabecular bone indirectly, provides similar information regarding bone quality when compared with micro-CT.

Abbreviations

UTE	ultra-short echo time
micro-CT	micro-computed tomography
T_E	echo time
D_k	fractal dimension
FOV	field of view
SPIR	spectral presaturation with inversion recovery
T_R	repetition time
ROI	region of interest
Po	porosity of the trabecular bone
Tr.Th	trabecular thickness
Tr.Se	trabecular separation
Tr.N	trabecular number
SAR	specific absorption rate

References

1. Arnett FC, Edworthy SM, Bloch DA, McShane DJ, Fries JF, Cooper NS, Healey LA, Kaplan SR, Liang MH, Luthra HS, Medsger TA, Mitchell DM, Neustadt DH, Pinals RS, Schaller JG, Sharp JT, Wilder RL, Hunder GG. The American Rheumatism Association 1987 revised criteria for the classification of rheumatoid arthritis. Arthritis Rheum. 1988; 31(3):315–324. [PubMed: 3358796]
2. Fleming A, Benn RT, Corbett M, Wood PH. Early rheumatoid disease. II. Patterns of joint involvement. Ann Rheum Dis. 1976; 35(4):361–364. [PubMed: 970995]
3. Fleming A, Crown JM, Corbett M. Incidence of joint involvement in early rheumatoid arthritis. Rheumatol Rehabil. 1976; 15(2):92–96. [PubMed: 935739]
4. Deodhar AA, Brabyn J, Jones PW, Davis MJ, Woolf AD. Longitudinal study of hand bone densitometry in rheumatoid arthritis. Arthritis Rheum. 1995; 38(9):1204–1210. [PubMed: 7575713]
5. Forsblad-d'Elia H, Carlsten H. Bone mineral density by digital X-ray radiogrammetry is strongly decreased and associated with joint destruction in long-standing rheumatoid arthritis: a cross-sectional study. BMC Musculoskelet Disord. 2011; 12:242. [PubMed: 22024200]
6. Haugeberg G, Strand A, Kvien TK, Kirwan JR. Reduced loss of hand bone density with prednisolone in early rheumatoid arthritis: results from a randomized placebo-controlled trial. Arch Intern Med. 2005; 165(11):1293–1297. [PubMed: 15956010]
7. Kazakia GJ, Hyun B, Burghardt AJ, Krug R, Newitt DC, de Papp AE, Link TM, Majumdar S. In vivo determination of bone structure in postmenopausal women: a comparison of HR-pQCT and high-field MR imaging. J Bone Miner Res. 2008; 23(4):463–474. [PubMed: 18052756]

8. Krug R, Carballido-Gamio J, Burghardt AJ, Kazakia G, Hyun BH, Jobke B, Banerjee S, Huber M, Link TM, Majumdar S. Assessment of trabecular bone structure comparing magnetic resonance imaging at 3 Tesla with high-resolution peripheral quantitative computed tomography ex vivo and in vivo. Osteoporos Int. 2008; 19(5):653–661. [PubMed: 17992467]
9. Phan CM, Matsuura M, Bauer JS, Dunn TC, Newitt D, Lochmueller EM, Eckstein F, Majumdar S, Link TM. Trabecular bone structure of the calcaneus: comparison of MR imaging at 3.0 and 1.5 T with micro-CT as the standard of reference. Radiology. 2006; 239(2):488–496. [PubMed: 16569786]
10. Majumdar S, Newitt D, Mathur A, Osman D, Gies A, Chiu E, Lotz J, Kinney J, Genant H. Magnetic resonance imaging of trabecular bone structure in the distal radius: relationship with X-ray tomographic microscopy and biomechanics. Osteoporos Int. 1996; 6(5):376–385. [PubMed: 8931032]
11. Vieth V, Link TM, Lotter A, Persigehl T, Newitt D, Heindel W, Majumdar S. Does the trabecular bone structure depicted by high-resolution MRI of the calcaneus reflect the true bone structure? Invest Radiol. 2001; 36(4):210–217. [PubMed: 11283418]
12. Wehrli FW, Ford JC, Attie M, Kressel HY, Kaplan FS. Trabecular structure: preliminary application of MR interferometry. Radiology. 1991; 179(3):615–621. [PubMed: 2027962]
13. Link TM, Majumdar S, Augat P, Lin JC, Newitt D, Lane NE, Genant HK. Proximal femur: assessment for osteoporosis with T2* decay characteristics at MR imaging. Radiology. 1998; 209(2):531–536. [PubMed: 9807585]
14. Wehrli FW, Hilaire L, Fernandez-Seara M, Gomberg BR, Song HK, Zemel B, Loh L, Snyder PJ. Quantitative magnetic resonance imaging in the calcaneus and femur of women with varying degrees of osteopenia and vertebral deformity status. J Bone Miner Res. 2002; 17(12):2265–2273. [PubMed: 12469921]
15. Robson MD, Gatehouse PD, Bydder M, Bydder GM. Magnetic resonance: an introduction to ultrashort TE (UTE) imaging. J Comput Assist Tomogr. 2003; 27(6):825–846. [PubMed: 14600447]
16. Springer F, Martirosian P, Schwenzer NF, Szimtenings M, Kreisler P, Claussen CD, Schick F. Three-dimensional ultrashort echo time imaging of solid polymers on a 3-Tesla whole-body MRI scanner. Invest Radiol. 2008; 43(11):802–808. [PubMed: 18923260]
17. Springer F, Steidle G, Martirosian P, Syha R, Claussen CD, Schick F. Rapid assessment of longitudinal relaxation time in materials and tissues with extremely fast signal decay using UTE sequences and the variable flip angle method. Invest Radiol. 2011; 46(10):610–617. [PubMed: 21577126]
18. Krug R, Larson PE, Wang C, Burghardt AJ, Kelley DA, Link TM, Zhang X, Vigneron DB, Majumdar S. Ultrashort echo time MRI of cortical bone at 7 tesla field strength: a feasibility study. J Magn Reson Imaging. 2011; 34(3):691–695. [PubMed: 21769960]
19. Wehrli FW, Song HK, Saha PK, Wright AC. Quantitative MRI for the assessment of bone structure and function. NMR Biomed. 2006; 19(7):731–764. [PubMed: 17075953]
20. Thiel W. Die Konservierung ganzer Leichen in natürlichen Farben [The preservation of the whole corpse with natural color]. Ann Anat. 1992; 174(3):185–195. [PubMed: 1503236]
21. Thiel W. Ergänzung für die Konservierung ganzer Leichen nach W. Thiel [Supplement to the conservation of an entire cadaver according to W. Thiel]. Ann Anat. 2002; 184(3):267–269. [PubMed: 12061344]
22. Haase A, Frahm J, Hanicke W, Matthaei D. ^{1}H NMR chemical shift selective (CHESS) imaging. Phys Med Biol. 1985; 30(4):341–344. [PubMed: 4001160]
23. Parfitt AM, Drezner MK, Glorieux FH, Kanis JA, Malluche H, Meunier PJ, Ott SM, Recker RR. Bone histomorphometry: standardization of nomenclature, symbols, and units. Report of the ASBMR Histomorphometry Nomenclature Committee. J Bone Miner Res. 1987; 2(6):595–610. [PubMed: 3455637]
24. Haire TJ, Hodgskinson R, Ganney PS, Langton CM. A comparison of porosity, fabric and fractal dimension as predictors of the Young's modulus of equine cancellous bone. Med Eng Phys. 1998; 20(8):588–593. [PubMed: 9888237]

25. Sanchez-Molina D, Velazquez-Ameijide J, Quintana V, Arregui-Dalmases C, Crandall JR, Subit D, Kerrigan JR. Fractal dimension and mechanical properties of human cortical bone. Med Eng Phys. 2013; 35(5):576–582. [PubMed: 22835437]
26. Weinstein RS, Majumdar S. Fractal geometry and vertebral compression fractures. J Bone Miner Res. 1994; 9(11):1797–1802. [PubMed: 7863830]
27. Chappard D, Legrand E, Haettich B, Chales G, Auvinet B, Eschard JP, Hamelin JP, Basle MF, Audran M. Fractal dimension of trabecular bone: comparison of three histomorphometric computed techniques for measuring the architectural two-dimensional complexity. J Pathol. 2001; 195(4):515–521. [PubMed: 11745685]
28. Armas LA, Akhter MP, Drincic A, Recker RR. Trabecular bone histomorphometry in humans with Type 1 Diabetes Mellitus. Bone. 2012; 50(1):91–96. [PubMed: 22001578]
29. Ding M, Odgaard A, Hvid I. Changes in the three-dimensional microstructure of human tibial cancellous bone in early osteoarthritis. J Bone Joint Surg Br. 2003; 85(6):906–912. [PubMed: 12931817]
30. Sornay-Rendu E, Boutroy S, Munoz F, Delmas PD. Alterations of cortical and trabecular architecture are associated with fractures in postmenopausal women, partially independent of decreased BMD measured by DXA: the OFELY study. J Bone Miner Res. 2007; 22(3):425–433. [PubMed: 17181395]
31. Barou O, Valentin D, Vico L, Tirode C, Barbier A, Alexandre C, Lafage-Proust MH. High-resolution three-dimensional micro-computed tomography detects bone loss and changes in trabecular architecture early: comparison with DEXA and bone histomorphometry in a rat model of disuse osteoporosis. Invest Radiol. 2002; 37(1):40–46. [PubMed: 11753153]
32. Lee AT, Williams AA, Lee J, Cheng R, Lindsey DP, Ladd AL. Trapezium trabecular morphology in carpometacarpal arthritis. J Hand Surg Am. 2013; 38(2):309–315. [PubMed: 23267754]
33. Xiang A, Kanematsu M, Mitamura M, Kikkawa H, Asano S, Kinoshita M. Analysis of change patterns of microcomputed tomography 3-dimensional bone parameters as a high-throughput tool to evaluate antiosteoporotic effects of agents at an early stage of ovariectomy-induced osteoporosis in mice. Invest Radiol. 2006; 41(9):704–712. [PubMed: 16896306]
34. Fouque-Aubert A, Boutroy S, Marotte H, Vilayphiou N, Bacchetta J, Miossec P, Delmas PD, Chapurlat RD. Assessment of hand bone loss in rheumatoid arthritis by high-resolution peripheral quantitative CT. Ann Rheum Dis. 2010; 69(9):1671–1676. [PubMed: 20525847]
35. Laan RF, van Riel PL, van de Putte LB, van Erning LJ, van't Hof MA, Lemmens JA. Low-dose prednisone induces rapid reversible axial bone loss in patients with rheumatoid arthritis. A randomized, controlled study. Ann Intern Med. 1993; 119(10):963–968. [PubMed: 8105737]
36. Eriksen EF, Eghbali-Fatourechi GZ, Khosla S. Remodeling and vascular spaces in bone. J Bone Miner Res. 2007; 22(1):1–6. [PubMed: 17040170]
37. Hawkins RA, Choi Y, Huang SC, Hoh CK, Dahlbom M, Schiepers C, Satyamurthy N, Barrio JR, Phelps ME. Evaluation of the skeletal kinetics of fluorine-18-fluoride ion with PET. J Nucl Med. 1992; 33(5):633–642. [PubMed: 1569473]
38. McCarthy I. The physiology of bone blood flow: a review. J Bone Joint Surg Am. 2006; 88(Suppl. 3):4–9. [PubMed: 17079361]
39. Reeve J, Arlot M, Wootton R, Edouard C, Tellez M, Hesp R, Green JR, Meunier PJ. Skeletal blood flow, iliac histomorphometry, and strontium kinetics in osteoporosis: a relationship between blood flow and corrected apposition rate. J Clin Endocrinol Metab. 1988; 66(6):1124–1131. [PubMed: 3372678]
40. Vogt MT, Cauley JA, Kuller LH, Nevitt MC. Bone mineral density and blood flow to the lower extremities: the study of osteoporotic fractures. J Bone Miner Res. 1997; 12(2):283–289. [PubMed: 9041062]
41. Wang YX, Griffith JF, Kwok AW, Leung JC, Yeung DK, Ahuja AT, Leung PC. Reduced bone perfusion in proximal femur of subjects with decreased bone mineral density preferentially affects the femoral neck. Bone. 2009; 45(4):711–715. [PubMed: 19555783]
42. Biswas R, Bae W, Diaz E, Masuda K, Chung CB, Bydder GM, Du J. Ultrashort echo time (UTE) imaging with bi-component analysis: bound and free water evaluation of bovine cortical bone subject to sequential drying. Bone. 2012; 50(3):749–755. [PubMed: 22178540]

43. Rad HS, Lam SC, Magland JF, Ong H, Li C, Song HK, Love J, Wehrli FW. Quantifying cortical bone water in vivo by three-dimensional ultra-short echo-time MRI. NMR Biomed. 2011; 24(7): 855–864. [PubMed: 21274960]
44. Techawiboonwong A, Song HK, Leonard MB, Wehrli FW. Cortical bone water: in vivo quantification with ultrashort echo-time MR imaging. Radiology. 2008; 248(3):824–833. [PubMed: 18632530]
45. Techawiboonwong A, Song HK, Wehrli FW. *In vivo* MRI of submillisecond T_2 species with two-dimensional and three-dimensional radial sequences and applications to the measurement of cortical bone water. NMR Biomed. 2008; 21(1):59–70. [PubMed: 17506113]
46. Bae WC, Chen PC, Chung CB, Masuda K, D'Lima D, Du J. Quantitative ultrashort echo time (UTE) MRI of human cortical bone: correlation with porosity and biomechanical properties. J Bone Miner Res. 2012; 27(4):848–857. [PubMed: 22190232]
47. Diaz E, Chung CB, Bae WC, Statum S, Znamirowski R, Bydder GM, Du J. Ultrashort echo time spectroscopic imaging (UTESI): an efficient method for quantifying bound and free water. NMR Biomed. 2012; 25(1):161–168. [PubMed: 21766381]
48. De Santis S, Rebuzzi M, Di Pietro G, Fasano F, Maraviglia B, Capuani S. *In vitro* and *in vivo* MR evaluation of internal gradient to assess trabecular bone density. Phys Med Biol. 2010; 55(19): 5767–5785. [PubMed: 20844335]
49. Capuani S. Water diffusion in cancellous bone. Microporous Mesoporous Mater. 2013; 178:34–38.
50. Rebuzzi M, Vinicola V, Taggi F, Sabatini U, Wehrli FW, Capuani S. Potential diagnostic role of the MRI-derived internal magnetic field gradient in calcaneus cancellous bone for evaluating postmenopausal osteoporosis at 3 T. Bone. 2013; 57(1):155–163. [PubMed: 23899635]
51. Unger S, Blauth M, Schmoelz W. Effects of three different preservation methods on the mechanical properties of human and bovine cortical bone. Bone. 2010; 47(6):1048–1053. [PubMed: 20736094]
52. Wilke HJ, Werner K, Haussler K, Reinehr M, Bockers TM. Thiel-fixation preserves the non-linear load–deformation characteristic of spinal motion segments, but increases their flexibility. J Mech Behav Biomed Mater. 2011; 4(8):2133–2137. [PubMed: 22098913]

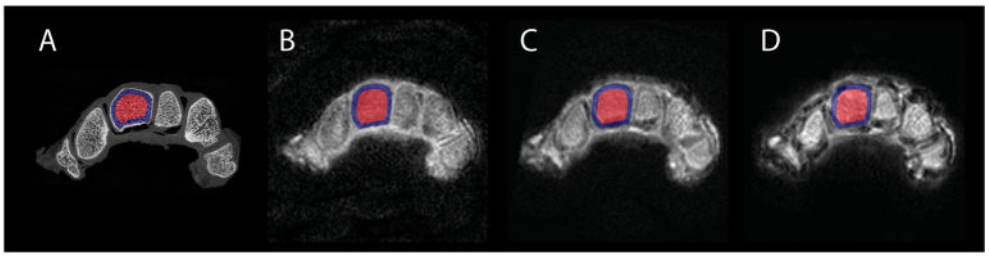

Figure 1.

Representative axial slices acquired with micro-CT (A), and with UTE MRI (T_E 150 μs) at 1.5 T (B), 3.0 T (C) and 7.0 T (D) after coregistration. Results of the coregistration procedure show no relevant spatial differences. Note the sample ROIs used for the capitate (red, center ROI; blue, subcortical ROI).

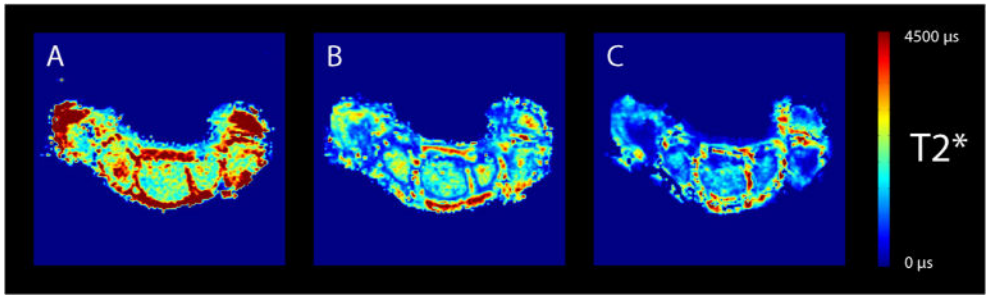

Figure 2.

Typical T_2* relaxation time maps obtained at 1.5 T (A), 3.0 T (B) and 7.0 T (C). Note the difference in T_2* relaxation time of trabecular bone at the different field strengths.

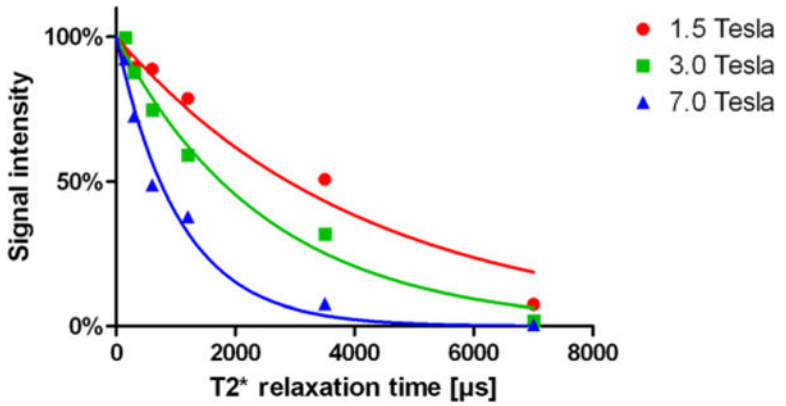

Figure 3.

Exemplary signal intensity decay and obtained fit curves for trabecular bone at different field strengths.

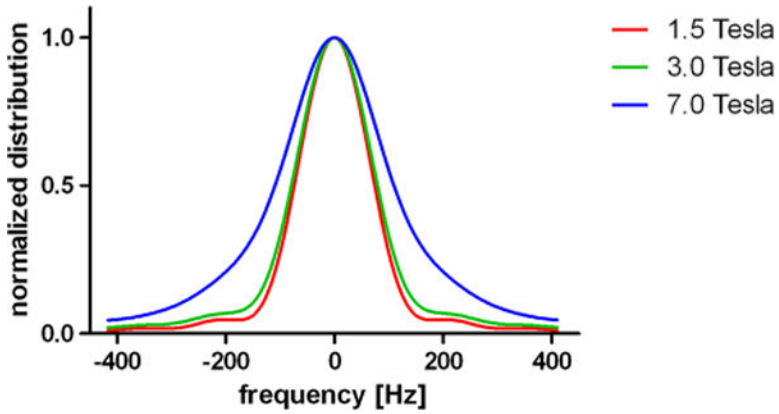

Figure 4.

Normalized frequency distribution within an exemplary ROI. Note the increase of the FWHM value with field strength (1.5 T, 156.25 Hz, 3 T, 169.27 Hz; 7 T, 221.35 Hz). Corresponding T_2* values within the same ROI were the following: 1.5 T, 4168 μs; 3 T, 2536 μs; 7 T, 1062 μs.

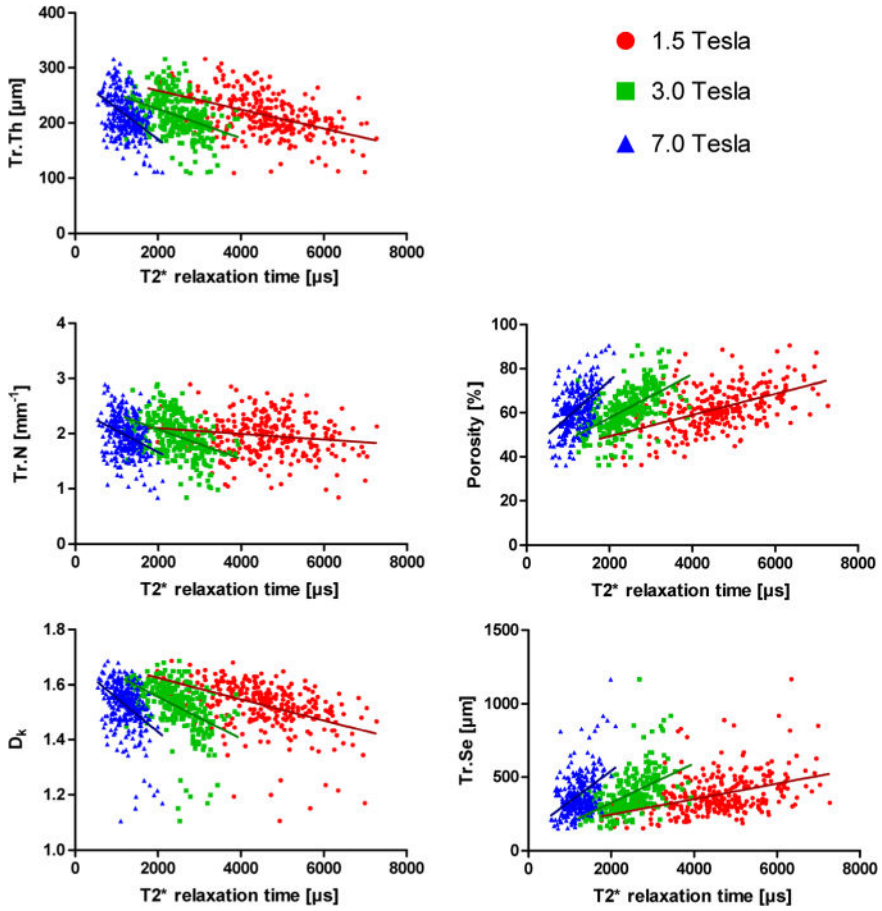

Figure 5.

Correlation analysis of T_2* relaxation time acquired at 1.5, 3.0 and 7.0 T with structural parameters acquired with micro-CT.

Table 1

T_2* relaxation time (μs) of carpal bones at 1.5, 3.0 and 7.0 T

	Scaphoid	Lunate	Capitate	Hamate	Trapezium	Trapezoid	Pisiform	Triquetrum
T_2* 1.5 T	4274 ± 789[a,b]	4468 ± 967[c]	3957 ± 1260[d,e,f]	4284 ±1170[g,h]	4988 ±1055[d]	5009 ± 881[a,e,g]	5198 ± 748[b,c,f,h]	4487 ± 731
T_2* 3.0 T	2252 ± 558[i]	2390±511	2233 ±562[j]	2314 ± 532	2682 ±496[i,j]	2535 ±625	2518 ±471	2404 ± 584
T_2* 7.0 T	1153 ± 348[b]	1151± 247[k]	1159 ± 267[l]	1139 ± 267[h]	1301 ±333	1205 ± 238	1401 ±318[b,h,k,l]	1232 ± 250

a, c, g, i, j, l Statistically significant difference, $p < 0.05$.

b, d, e, f, h, k Statistically significant difference, $p < 0.01$.

Table 2

Structural parameters of carpal bones acquired with micro-CT

	Scaphoid	Lunate	Capitate	Hamate	Trapezium	Trapezoid	Pisiform	Triquetrum
Po (%)	58.1 ±10.1^{a,b}	61.8 ±6.7^{c}	56.3 ± 7.4^{d,e,f}	57.4 ±12.0^{g,h,i}	66.1 ±8.0^{a,d,g}	64.5 ± 5.9^{e,h}	68.6 ±11.3^{b,c,f,i,j}	61.7 ± 7.7^{j}
Tr.Th (μm)	220 ± 36^{b}	214 ±29^{k,l}	243 ± 35^{d,e,f,k}	229 ±32^{i,m}	203 ± 28^{d,m,n}	214 ±30^{e,o}	174 ± 35^{b,f,i,l,n,o,p}	219 ± 35^{p}
Tr.Se (μm)	325 ±110^{b,q}	362 ± 95	323 ± 85^{f,r}	353 ± 167	431 ±134^{q,r}	411 ±81	451 ± 229^{b,f}	388 ± 103
Tr.N (mm^{-1})	2.32 ± 0.31^{q,s}	2.21 ±0.34	2.24 ±0.35	2.24 ±0.46	2.04 ± 0.37^{q}	2.03 ±0.24^{s}	2.13 ±0.49	2.12 ±0.29
D_k	1.55 ± 0.07^{a,b}	1.54 ± 0.05^{l,t}	1.58 ±0.05^{d,f,u}	1.56 ± 0.08^{g,i}	1.48 ±0.11^{a,d,g,t}	1.52 ±0.05^{o,u}	1.44 ±0.12^{b,f,i,l,o,p}	1.53 ± 0.07^{p}

a, b, d, e, f, g, i, k, l, n, o, p Statistically significant difference, $p < 0.01$.

c, h, j, m, q, r, s, t, u Statistically significant difference, $p < 0.05$.